J Polym Res (2007) 14:431–439
DOI 10.1007/s10965-007-9115-9

Novel nanocomposite of epoxy resin by introduced reactive and nanoporous material

Chao-Chen Yang · Feng-Chih Chang · Yen-Zen Wang · Chia-Ming Chan · Chen-Lung Lin · Wen-Yi Chen

Received: 10 October 2006 / Accepted: 29 April 2007 / Published online: 12 October 2007
© Springer Science + Business Media B.V. 2007

Abstract A reactive and nanoporous particle (OG) was introduced to UV-cured epoxy resin to form great low D_k material for electronic industrial. We expected the porous cage of OG to decrease the dielectric constant of UV-cured epoxy resin and multiple reactive functional groups (oxirane ring) of OG reacted with photoinitiator to increase the curing density of UV-cured epoxy resin. The glass transition temperatures (T_g) of epoxy increases with the increase of the OG content up to 10 phr due to the increase of crosslinking density. Excessive aggregation at highest OG content of 15 phr results in the reduced crosslinking density and T_g. The char yield of the composite increases with increase of OG content because stable Si and SiO_2 are formed after thermal decomposition. The presence of OG results in the higher porosity and thus the lower dielectric constant.

Keywords POSS · Dielectric constant · Thermal properties · Epoxy resin · Nanocomposites

C.-C. Yang · Y.-Z. Wang
Department of Chemical Engineering,
National Yun-Lin University of Science and Technology,
640 Yun-Lin, Taiwan

F.-C. Chang · C.-M. Chan · C.-L. Lin
Institute of Applied Chemistry, National Chiao Tung University,
300 Hsinchu, Taiwan

W.-Y. Chen (✉)
Division of Advanced Fiber Materials and Applications,
Industrial Technology Research Institute,
300 Hsinchu, Taiwan
e-mail: teddyc.ac86g@nctu.edu.tw

Introduction

Because of their suitable mechanical strength, favorable viscous properties, light weight and low cost, filled epoxy materials have been widely used in microelectronic packages as molding compounds to encapsulate semiconductor devices, as underfill materials to reinforce the strength of solder joints, and as die attach adhesives to bond silicon chips onto substrates. The use of filled epoxy materials introduces many interfaces and makes packages more complex.

The polyhedral oligomeric silsesquioxanes (POSS) as modifiers of organic polymers have received a great deal of attention recently. One special feature of POSS particles of about 1.5 nm in diameter is comparable to that of polymer segments. Incorporation of POSS particles into linear thermoplastics or thermoset networks can be used to modify the structure in nano-scale. These modifications can ultimately affect the thermal, oxidative, and dimensional stabilities of many polymers and upgrade their properties for numerous high performance applications as engineering plastics. These enhancements have been applied to a wide range of thermoplastics and a few thermoset systems, i.e. methacrylates [1, 2], styrenes [3], norbornenes [4], epoxies [5–10], and siloxanes [11] etc. It has been reported that the monofunctional or multifunctional POSS-epoxy can be incorporated into the backbone of epoxy resin to improve its thermal properties [5–10].

Ultraviolet (UV) radiation curing of polymer coatings has recently been dominated by the photoinitiated radical polymerization process, due partly to the thermal instability of early cationic system like aryldiazonium salt. With the advent of more stable alternatives, such as the onium salt, the cationic polymerization process has become important

because of the several significant advantages it possesses over the radical polymerization. The main advantage is its ability to allow spontaneous cure reaction in the presence of oxygen, providing significant advantage in coatings in contrast to the radical polymerization. Typical onium-based epoxy systems respond well throughout the UV-near visible spectral region. Mechanisms for the cationic-based cure initiation and propagation have been discussed in details previously [12, 13]. The onium salt is decomposed initially by the UV exposure into cations and a photosensitive acid, leading to liberation of an electron-deficient fragment as the polymerization initiator to induce the polymerization.

Epoxy resins have many features such as low shrinkage, good chemical resistance, outstanding adhesion and high electrical insulation that have been widely applied in microelectronics (packaging materials of microelectronics and PCB). The need for materials with lower dielectric constant become more stringent as the size of electronic devices is reduced to avoid cross talk between conducting wires. Further expounding on the RC time delay, the delay timeτcan be approximate as by Eq. 1 [14]:

$$\tau = RC = 2\rho\varepsilon\varepsilon_0\left[\frac{4L^2}{P^2} + \frac{L^2}{T^2}\right] \quad (1)$$

where τ is the sign delay time, R is the resistance, C is the capacitance, ρ is the specific resistance of the conductor, ε is the dielectric constant of the insulating material, ε_0 is the dielectric constant of the vacuum, L is the length of the conductor, P is the distance between two conducting lines, and T is the thickness of the conductor. Based on Eq. 1, higher sign speed can be obtained in three ways [15]: changing the layout and/or the ratio of width to thickness of the metal lines, decreasing the specific resistance of the interconnect metal, and decreasing the dielectric constant of the insulating material (internet dielectric). In this investigation, we focus on decreasing the dielectric constant of the insulating material. There are many methods to decrease the dielectric constant of insulating materials [16–20]. We introduce the nanoporous particles into the insulating material to reduce the dielectric constant of the epoxy resin because of the incorporated nanoporous POSS owns a cube structure with diameter of 1.5 nm.

In the previous study, we prepared nanocomposite based on OG/m-phenyl diamine (D_k=2.3, T_g=239 °C) with low dielectric constant and high thermal properties [21]. In this investigation, we used various multifunctional POSS-epoxy (OG) compositions in the UV-cured epoxy resin. We expected that the OG can be incorporated into the backbone of the epoxy resin upon UV curing. We expect to obtain a lower composition of OG for the significant reduction of the dielectric constant and the improved thermal properties of the UV-cured epoxy resin. The specific focus of this investigation is placed on the thermal and dielectric properties by DMA, TGA, and DEA, respectively.

Experimental

Materials

The octakis(dimethylsiliyloxy)silsesquixoxane ($HMe_2SiOSiO_{1.5})_8$ and platinum 1,3-divinyl-1,1,3,3-tetramethyl-disiloxane [Pt(dvs)] were purchased from Aldrich of USA. The allyl glycidyl ether (AGE) was purchased from Acros of Belgium. The DGEBA (DER 331, EEW=190 g/eq.) was purchased from Dow Chemical Company of USA. The triarylsulfonium hexafluoroantimonate (UVI 6974, photoinitiator) was purchased from Union Carbide Company of USA. Structures of chemicals employed in this study are illustrated in Scheme 1.

Octakis(dimethylsiloxypropylglycidyl ether)silsesquioxane (OG) [6]

The preparation of POSS-epoxy (OG) was carried out by adding $(HMe_2SiOSiO_{1.5})_8$ (0.50 g, 0.49 mmol) into a magnetically stirred 25 ml Schlenk flask. Toluene (5 ml) was added and the solution was stirred for 5 min. AGE (0.46 ml, 3.92 mmol) was then added, followed by 10 drops of 2.0 mM Pt(dvs). The reaction mixture was stirred for 8 h at 50 °C, cooled, and 0.5 g of dry activated charcoal was added. After stirring for 10 min, the mixture was filtered through a 0.45 μm Teflon membrane into a vial and stored as a clear solution of 10 wt%. Removal of solvents affords an opaque viscous liquid with a yield of 0.86 g (90%). The general synthetic reaction of OG is shown in Scheme 2.

Photopolymerization

Table 1 shows the codes and compositions used in this study. A typical process of photopolymerization was carried out by placing the mixture of sample onto a glass plate at a typical thickness of 300 μm. A 180 W medium-pressure arc lamp (λmax=366 nm) irradiated the sample at a distance of 10 cm for 70 min at room temperature. The uv-cured sample was then heated at 180 °C for 120 min (post-cured).

Characterizations

Fourier transform infrared spectra (FT-IR)

The sample was placed on a KBr pellet and FTIR spectra were obtained by using a Nicolet AVATAR 320 FT-IR (Madison, Wisconsin, USA) operating at a resolution of 2 cm^{-1}.

Scheme 1 Chemical structures of compounds used in this study

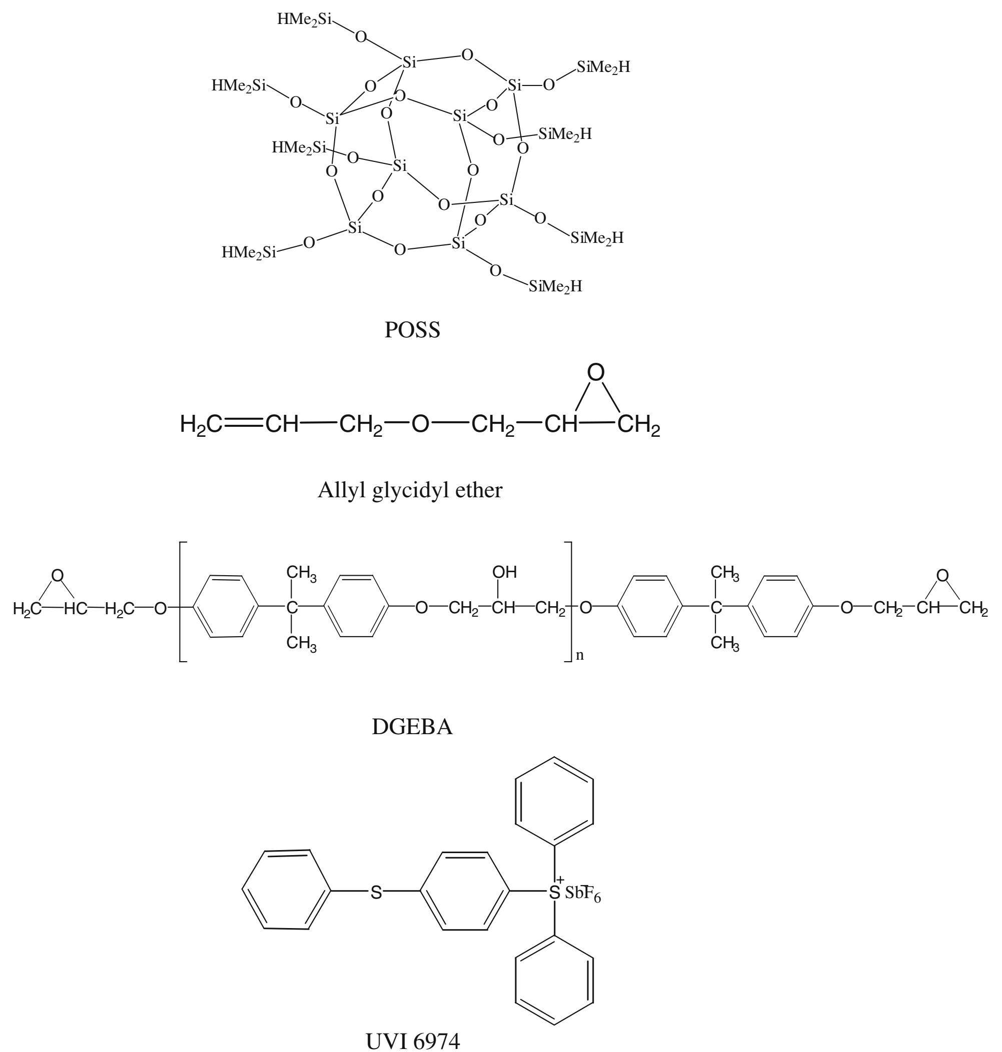

^{1}H NMR

All solutions were prepared by dissolving samples in $CDCl_3$. ^{1}H NMR experiments were performed at 500 MHz by using a Bruker AMX-500 FT NMR Spectrometer.

Dynamic mechanical analyzer

Dynamic mechanical measurements were carried out on a DuPont dynamic mechanical analyzer (DMA 2980). The clamp model was a single cantilever with frequency of 1 Hz

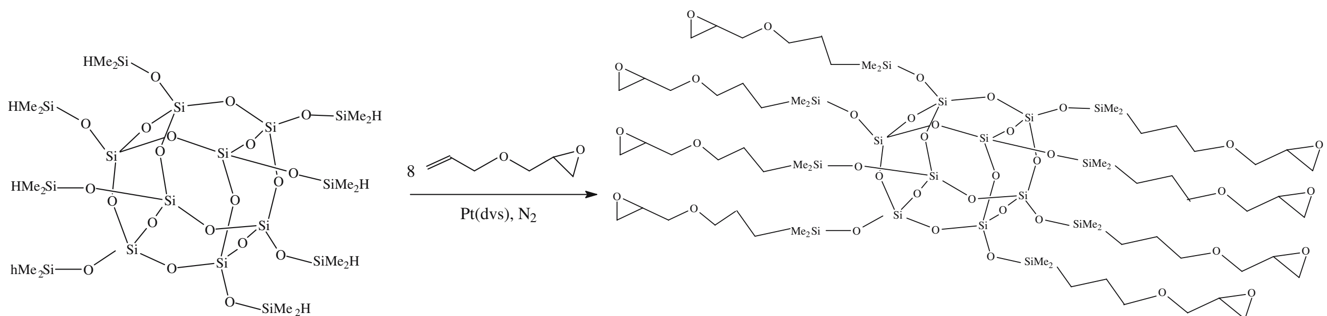

Scheme 2 OG synthesis step

Table 1 Codes and compositions of materials prepared in this study

Codes	Components
A0	DGEBA : UVI 6974 : OG=100 : 5 : 0 (phr)
A3	DGEBA : UVI 6974 : OG=100 : 5 : 3 (phr)
A5	DGEBA : UVI 6974 : OG=100 : 5 : 5 (phr)
A10	DGEBA : UVI 6974 : OG=100 : 5 : 10 (phr)
A15	DGEBA : UVI 6974 : OG=100 : 5 : 15 (phr)

and the heating rate was 3 °C/min from 40 to 195 °C. The specimen dimensions are ca. 17.5×11.5×2.8 mm.

Thermo-gravimetric analyzer

Thermal stability studies were carried out using a DuPont thermo-gravimetric analyzer (TGA 2050) performed under a nitrogen or air atmosphere. The cured sample (ca. 7 mg) was placed in a Pt cell and heated at a rate of 20 °C/min from 30 to 750 °C with a nitrogen or air flow of 90 ml/min, respectively.

Dielectric analysis (DEA)

DEA experiments were performed using a Du-Pont 2970 Dielectric Analyzer equipped with a ceramic parallel plate sensor. The frequency used for the DEA experiments was 100 kHz and the permittivity (ε') was monitored.

Density determination

The measured densities (d^{M}) of DGEBA/OG system were obtained by dividing the weight of the films by their volume. At least three specimens were used for each density data point. The relative porosity increase was calculated based on Eq. 2.

$$\text{Relative}-\text{porosity}-\text{increase}(\phi_r) = \left[\left(d^{\mathrm{T}}-d^{\mathrm{M}}\right)/d^{\mathrm{T}}\right]\times 100\% + (0.048\times \mathrm{V}\%) \qquad (2)$$

where d^{T} is the theoretical density of the DGEBA-UVI 6974-OG system estimated from the weight percentage of OG in the nanocomposite and the density of OG and epoxy (1.23 and 1.35 g/cm^3, respectively). V % is the volume percentage of OG in the nanocomposites.

Morphology

The scanning electron microscope (SEM) observations were performed on a JEOL 5300 apparatus. The samples were fractured in liquid nitrogen and the fracture surfaces were contrasted with gold. Samples for the transmission electron microscopy (TEM) study and the samples were micro-tomed with a Leica Ultracut Uct into about 90 nm thick slices. Subsequently, a layer of carbon about 3 nm thick was deposited onto these slices and placed on mesh 200 copper nets for TEM observation. The TEM instrument is a JEOL-2000 FX, with an acceleration voltage of 200 kV.

Results and discussion

Characteristic of chemical structure of OG

The cube structure of OG was characterized by FTIR. The characteristic IR absorption behavior of OG is summarized in Table 2. The FTIR spectra of the pure POSS, AGE, and OG (POSS-epoxy) are shown in Fig. 1. Figure 1a shows a sharp, strong, and symmetric Si–O–Si stretching peak at ~1,100 cm^{-1} corresponding to the silsequioxane cage and a relatively smaller Si–H stretching peak [22, 23] at ~2,140 cm^{-1}. The consistent presence of this peak demonstrates that the cube structure survives during processing. If the cube structure were degraded, one would observe a shift to asymmetric broad peaks of typical silica [23–25]. The AGE shows a small CH_2=CH– stretching peak at ~1,640 cm^{-1} and an epoxy ring asymmetric stretching peak at ~915 cm^{-1} as shown in Fig. 1b. Figure 1c shows that both Si–H and CH_2=CH peaks disappeared, implying that the allyl group of AGE has reacted with Si–H of POSS to create a covalent bonding in the POSS structure while the epoxy ring peak is still present on Fig. 1c [6]. The structure identification of OG for Choi [6] was conformed by a diffuse reflectance FTIR, in this study; we applied the ^{1}H– NMR to identify the chemical structure of OG. Figure 2a shows the chemical shifts of ^{1}H NMR of POSS for –CH_3 at 0.11 ppm and –Si–H group at 4.71 ppm. Figure 2b shows the chemical shifts of the AGE for the CH_2=CH– at 5.63, 5.01, and 4.92 ppm, respectively. Figure 2c shows the chemical shifts of the OG where the CH_2=CH– of AGE is converted to –CH_2–CH_2– of OG and the chemical shift of 5.63, 5.01, and 4.92 ppm shift to 0.57

Table 2 Characteristic absorptions of OG [23]

Functional group	Wavenumber (cm^{-1})	[a]Vibration type
Si–H	~2,200	ν_s
Si–H	800–900	δ_s
Si–C	1,250	ν_s
Si–O–Si	1,030–1,100	ν_s
C–H, aliphatic	2,840–3,000	ν_s ν_{as}
C–H, aliphatic	1,370–1,450	δ_s
C–H, aliphatic	1,150–1,350	ω τ
Epoxy ring	1,250	ν_s
Epoxy ring	810–950	ν_s
Epoxy ring	750–840	ν_s 12 μ band
C–H in Epoxy ring	2,990–3,050	ν_s

[a] ν_s symmetric vibration; ν_{as} asymmetric vibration; δ_s in-plane bending (scissoring); ω out-of-plane bending (wagging); τ out-of plane bending (twisting).

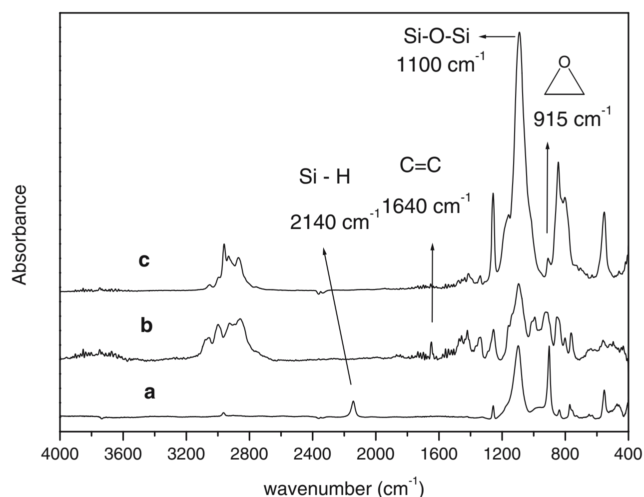

Fig. 1 FTIR spectra of **a** POSS, **b** AGE and **c** OG

and 1.60 ppm. The –Si–H of POSS chemical shift of 4.71 ppm disappeared in Fig. 2c. FTIR and ^{1}H NMR results positively identify the OG chemical structure, indicating that the POSS is able to react with AGE through hydrosilation to form the OG.

Thermal properties

We introduced the OG in the epoxy resin to increase its crosslinking density. Both DMA and TGA measurements were performed on cured epoxies containing 0, 3, 5, 10, and 15 phr of OG.

Glass transition temperature (Tg)

The glass transition temperature of DGEBA/OG composite was characterized by DMA. DMA for obtaining more accurate T_g and thus provides more detail information on the microstructure of the cured epoxy resin. For an epoxy resin, a depression in modulus over the glass transition region is observed. The diagram of tan δ versus temperature for a cured epoxy gives a major relaxation transition, corresponding to the T_g of the cured epoxy resin. Movement of chain segments in epoxy structure have a profound effect on the loss factors (tan δ and loss modulus) in the dynamic mechanical properties. The tan δ value of the α-peak (the glass transition) is of greater magnitude than that of the dispersion peak at lower temperatures, and is accompanied by the huge decrease in dynamic modulus with increasing temperature. Figure 3 shows the tan δ of DMA thermograms of cured epoxies containing various amount of OG. The temperature of tan δ of UV-cured epoxy resin is 143.3 °C. The trend clearly shows that the glass transition temperature increases with the increase of the OG content up to 10 phr (156.4 °C). However the T_g of the epoxy containing 15 phr (154.3 °C) of OG is actually

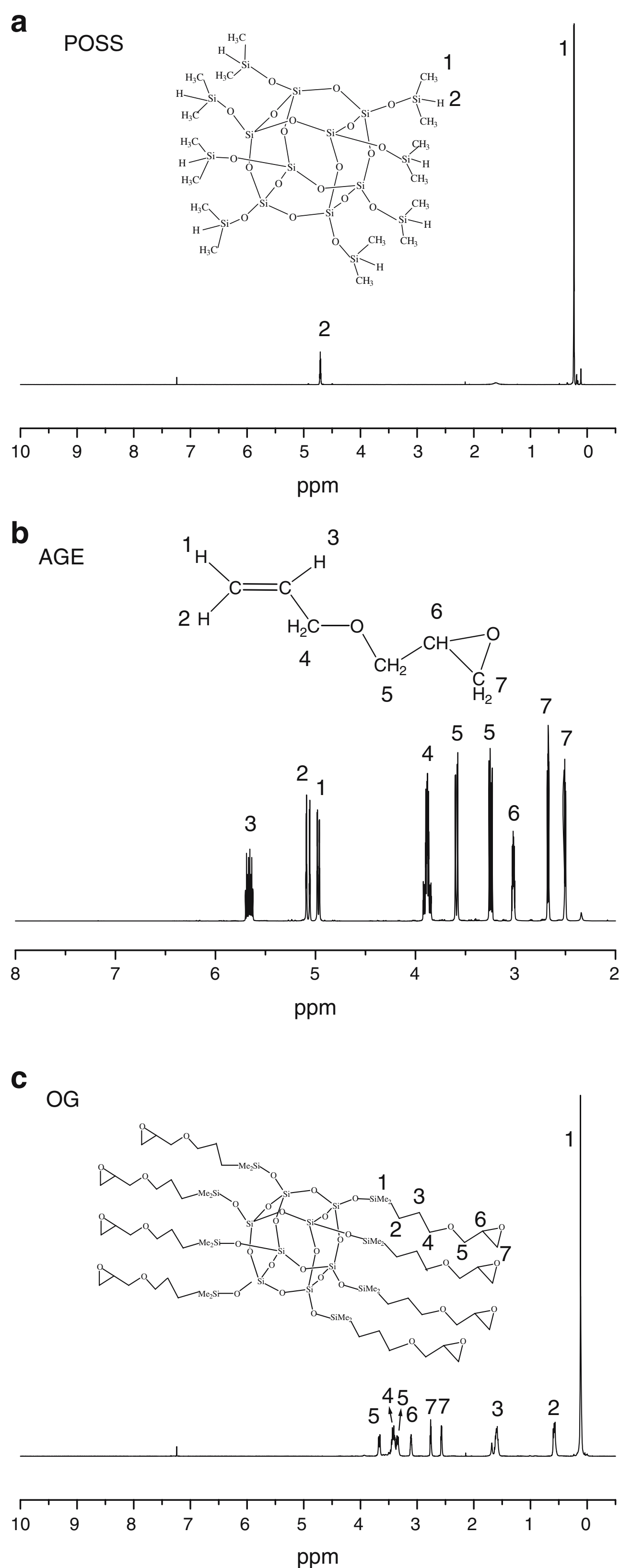

Fig. 2 ^{1}H NMR spectra of **a** POSS, **b** AGE and **c** OG

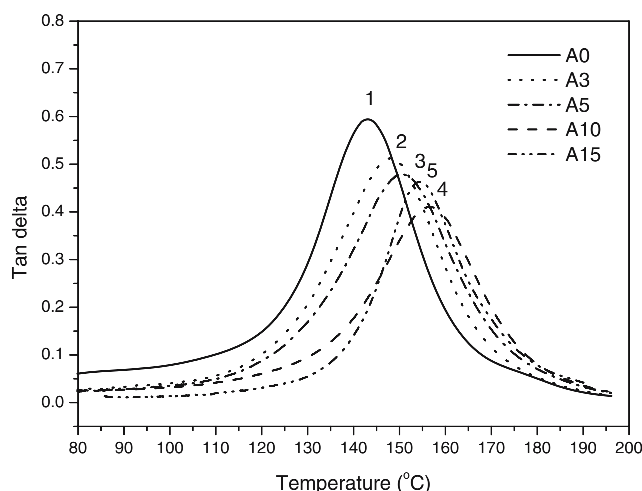

Fig. 3 Tan δ of DMA thermograms of uv-cured DGEBA/OG composites

decreased. The T_g data are listed in Table 3. It suggests that the incorporation of POSS cages into the epoxy network is able to hinder the movement of the network and results in a higher T_g as expected. The multifunctional epoxy groups of OG tend to increase the crosslinking density of the network and thus a higher T_g [5, 8, 10]. When the OG content is 15 phr (sample A15), OG molecules themselves tend to agglomerate into big domains during progress of curing and thus reduce overall degree of crosslinking and their T_gs. On the other hand, the peak height of Tan δ in DMA can be used to determine the crosslinking density since the loss tangent is sensitive to the degree of crosslinking. At temperatures well above T_g, the damping decreases with increasing degree of crosslinking [26]. The temperature of tan δ of DGEBA/OG nanocomposite with lower OG content (up to 10 phr OG) shifts to higher one, but higher OG content (15 phr OG) shifts to lower one. The peak height of Tan δ of DGEBA/OG nanocomposite was decreased with increasing of OG content up to 10 phr. However the peak height of tan δ of DGEBA/OG nanocomposite with 15 phr of OG is actually increased. We conformed that the crosslinking density of DGEBA/OG nanocomposite increased with increasing of OG content up to 10 phr, the lower crosslinking density of higher OG content (15 phr) was decreased. We believe that the decreasing of crosslinking density at high OG content is due to the dramatically aggregated POSS. Later, morphological characterizations will provide more evidences on the molecular aggregation of OG.

Table 3 Thermal properties of DGEBA-UVI 6974-OG system

Code	T_g (°C)	T_{dec} (°C, 5% loss)	Char yield (%) at 700 °C
A0	143.3	383.2	13.4
A3	148.3	379.4	15.7
A5	151.4	379.6	18.4
A10	156.4	383.5	21.5
A15	154.3	383.1	23.3

Thermal stabilities

The thermal stabilities evaluated by TGA in nitrogen are shown in Fig. 4 and the results are listed in Table 3. For a comparison of the relative thermal stabilities of composites, temperatures of 5% mass loss were selected as the degradation temperature (T_{dec}). TGA thermograms of epoxy resin with different OG contents under a N_2 atmosphere are shown in Fig. 4 and Table 3. The T_{dec} temperatures show very little difference. The char yield increases with increasing OG content unexpectively. When the cubic POSS structure is thermally degraded, residual silica and SiO_2 are usually formed. Therefore, greater OG content results in higher char yield [6, 23].

Morphology

The SEM and TEM were applied to observe the morphology of the DGEBA/OG nanocomposite. Figure 5a–d display the SEM micrographs of various compositions of OG with epoxy resin. The particle size is 30–50 nm and slight aggregation was found for those with lower OG contents. For the higher OG content (A15, OG 15 phr), dramatic aggregation was observed. The dramatic OG aggregation in epoxy resin matrix due to the poor miscibility tends to reduce the curing extent of the cross-linked network and results in a low T_g. Figure 6 displays the EDS photograph that can be used to confirm the particle aggregation of the POSS structure. The EDS photograph of red mark demonstrated high Si intensity. We confirmed the particle aggregation in DGEBA/OG nanocomposite to be a

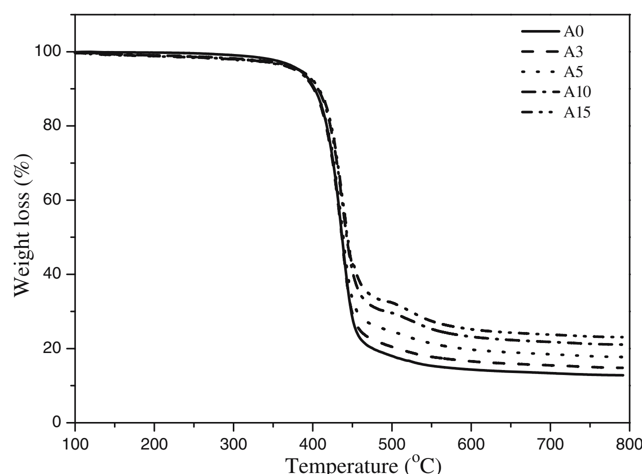

Fig. 4 TGA thermograms of uv-cured DGEBA/OG composites under N_2 atmosphere

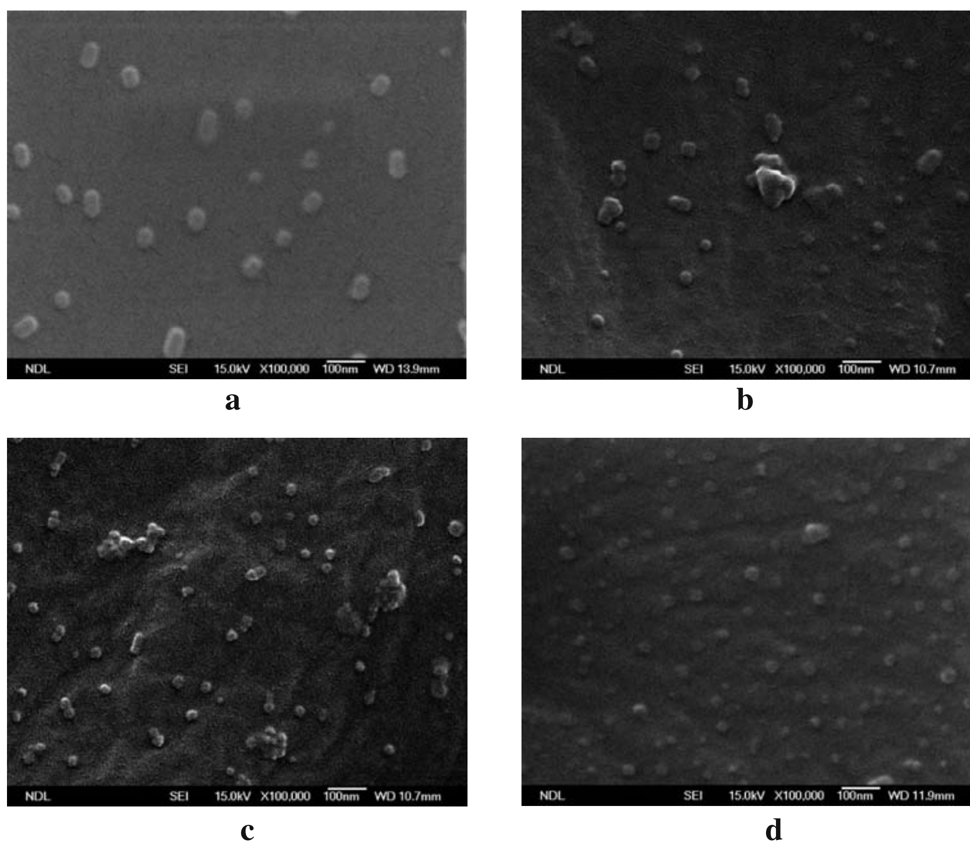

Fig. 5 SEM micrographs of uv-cured DGEBA/OG composites: **a** A3=3 phr, **b** A5=5 phr, **c** A10=10 phr, **d** A15=15 phr

POSS aggregation since POSS contained Si element in the DGEBA/OG nanocomposite. On the other hand, we can see that the morphology of POSS aggregation of network system is different to that of the non-network system. Many papers [27–29] reported that the POSS aggregation is able to self assemble to form an ordered structure from non-network system. In the network system, we found that the POSS aggregation is toward to adopt a particle-like structure not an ordered one. For network polymer with higher POSS content, the T_g is depressed due to the dramatic aggregation of POSS and the decreased cross-linking density. Figure 7 displays a TEM micrograph of DGEBA/OG nanocomposite with 10 phr of OG. We observed a disorder POSS aggregation structure in DGEBA/OG nanocomposite and the particle size is 30–50 nm similar to the SEM observation.

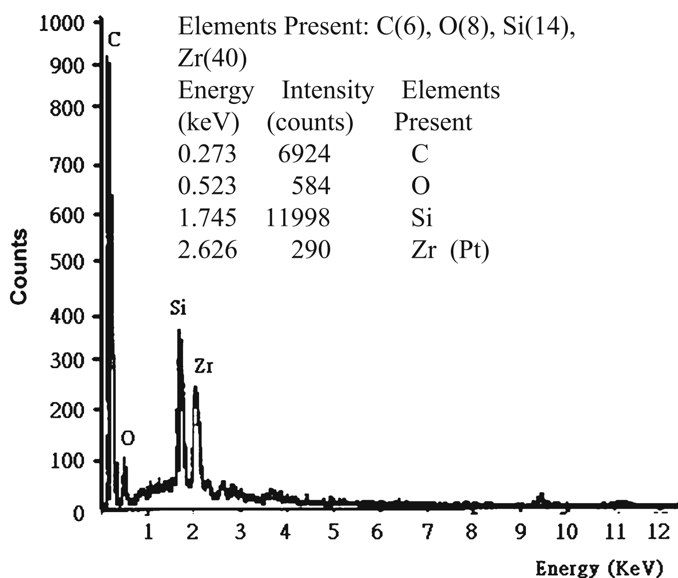

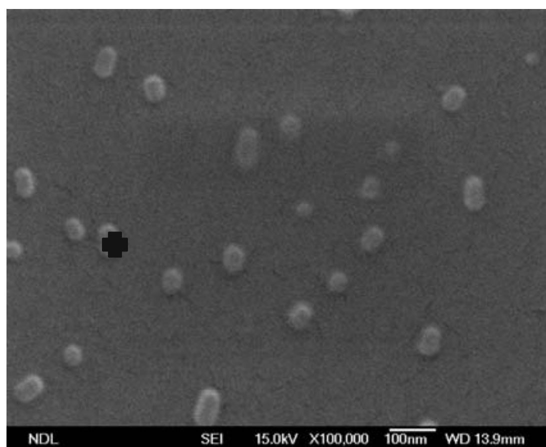

Fig. 6 The EDS spectrum and SEM micrograph of uv-cured DGEBA/OG containing 3 phr OG

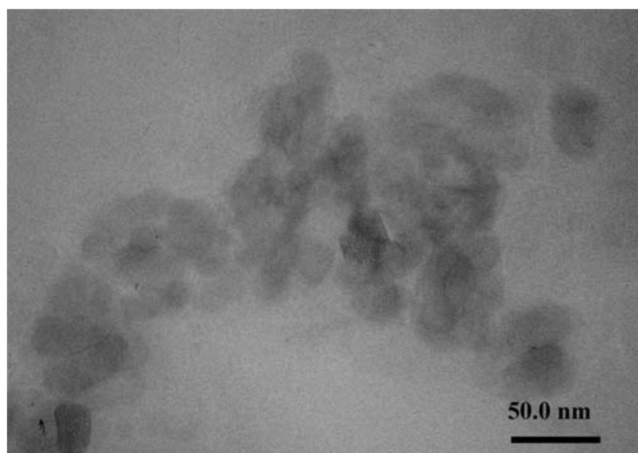

Fig. 7 TEM micrographs of uv-cured DGEBA/OG containing 10 phr OG

Dielectric property

Dielectric constants of the epoxy resins containing OG were measured at 100 kHz by DEA and the results of DEA and composite densities are summarized in Table 4. The dielectric constant of plain epoxy resin is about 3.71. The results show the dielectric constant of the DGEBA/OG nanocomposite decreases steadily with the increase of the OG (15 phr OG is 2.83). Many papers reported that polymer possessed a nanoporous structure that can effectively decrease the dielectric constant of a polymer [30, 31], due to the low dielectric constant (D_k of air is 1.1) of a porous structure. The reduction in the dielectric constant of the DGEBA/OG can be explained the presence of the porous cage of the OG and the increasing free volume of DGEBA/OG with OG content. Both the rigid, large nature of OG and the lightly aggregated structure of the DGEBA/OG nanocomposite contribute to the increase of the free volume of epoxy resin. The density measurement of DGEBA/OG nanocomposite was applied to determine the porosity of the DGEBA/OG nanocomposite. Since the porous structures of the nanocomposite films are difficult to obtain, we provided a simple method to compare the relative porosities of nanocomposite films. Equation 2 was used to calculate the relative porosity increase (ϕ_r) of the DGEBA/OG nanocomposite. The relative porosity increase (ϕ_r) is defined as the increased external porosity due to the introduction of POSS molecules in epoxy resin without considering the nanoporosity of POSS molecules themselves, that is calculated by Eq. 1 in the "Characterization section." The density of the neat resin is 1.35 g/cm^3 and the density of DGEBA/OG nanocomposite decreases with the increase of OG content (A15 is 1.12 g/cm^3). The relative-porosity-increase (ϕ_r) of the DGEBA/OG nanocomposite increases with the increase of OG content. The reduction of ϕ_r is partially due to the presence of the nanoporosities in the core of POSS structure [27, 32]. The external porosity of the DGEBA/OG system was introduced by tethering OG to epoxy resin. In this study, we introduced OG in a UV-cured epoxy system to form the network structure of the DGEBA/OG nanocomposite. The OG structure created higher free volume in epoxy resin contributing to the decrease of the dielectric constant of epoxy resin.

Conclusion

A new series of UV-cured nanocomposites of epoxy resin containing POSS-epoxy were investigated. The glass transition temperatures (T_g) of epoxy increases with the increase of the OG content up to 10 phr due to the increase of crosslinking density. Due to the poor miscibility between OG and epoxy, the OG component tends to phase-separate and aggregate during curing, especially at high OG content. Excessive aggregation at the maximum OG content of 15 phr results in reduced crosslinking density and T_g. The char yield of the composite increases with increasing of OG content because the stable Si and SiO_2 are formed after thermal decomposition. The presence of OG results in higher porosity and thus lower dielectric constant.

Table 4 Dielectric property and density of DGEBA-UVI 6974-OG system

	Dielectric permittivity at 25 °C	Theoretical density[a] (d^T) (g/cm^3)	Measured density (d^M) (g/cm^3)	Relative-porosity-increase (φ_r, %)	Density of epoxy resin in nanocomposite (dN) (g/cm^3)
A0	3.71±0.03	1.35	1.35	0	1.35
A3	3.35±0.02	1.35	1.25	7.14	1.25
A5	3.11±0.04	1.34	1.23	9.67	1.23
A10	2.95±0.02	1.34	1.20	10.33	1.20
A15	2.83±0.01	1.33	1.15	14.14	1.13

[a] Theoretical density (d^T): estimated from the weight percentage of OG in the nanocomposite and the density of OG and Epoxy (1.23 and 1.35 g/cm^3)

References

1. Lichtenhan JD, Otonari YA, Carr MJ (1995) Macromolecules 28:8435
2. Pyun J, Matyjaszewski K (2000) Macromolecules 33:217
3. Haddad TS, Lichtenhan JD (1996) Macromolecules 29:7302
4. Math PT, Jeon HG, Romo-Uribe A, Haddad TS, Lichtenhan JD (1999) Macromolecules 32:1194
5. Lee A, Lichtenhan JD (1998) Macromolecules 31:4970
6. Jiwon C, Jason H, Albert FY, Quan Z, Richard ML (2001) J Am Chem Soc 123:11420
7. Maria JA, Luis B, Diana PF, Roberto JJW (2003) Macromolecules 36:3128
8. Li GZ, Wang L, Toghiani H, Daulton TL, Pittman CU Jr (2002) Polymer 43:4167
9. Ramirez C, Abad MJ, Barral L, Cano J, Diez FJ, Lopez J, Montes R, Polo J (2003) J Therm Anal Calorim 72:421
10. Li GZ, Wang L, Ni HL, Pittman CU Jr (2001) J Inorg Organomet Polym 11:123
11. Lichtenhan JD, Vu NQ, Carter JA, Gilman JW, Feher FJ (1993) Macromolecules 26:2141
12. Dreyfuss MP (1965) Polymer 6:93
13. Pappas SP (1981) J Radiat Curing 8:28
14. Bohr MT (1996) Solid State Technol 9:105
15. Maier G (2001) Prog Polym Sci 26:3
16. Carter KR, DiPietro RA, Sanchez MI, Swanson SA (2001) Chem Mater 13:213
17. Huang QR, Volksen W, Huang E, Toney M, Frank CW, Miller RD (2002) Chem Mater 14:3676
18. Oh W, Park YH, Ree M, Chu SH, Char K, Lee JK, Kim SY (2003) Polymer 44:2518
19. Watkins JJ, Blackburn JM, McCarthy TJ (1999) Chem Mater 11:213
20. Zhang MC, Kang ET, Neoh KG, Tan KL (2000) Langmuir 16:9666
21. Chen WY, Wang YZ, Kuo SW, Huang CF, Tung PH, Chang FC (2004) Polymer 45:6897
22. Marcolli C, Calzaferri G (1999) Appl Organomet Chem 13:213
23. Wallace WE, Guttman CU, Antoucci JM (2000) Polymer 41:2219
24. Silverstein RM, Webster FX (1996) Spectrometric identification of organic compounds. Wiley, New York
25. Chen Y, Iroh JO (1999) Chem Mater 11:1222
26. Murayama T (1978) Dynamic mechanical analysis of polymeric material. Elsevier, New York
27. Leu CM, Reddy GM, Wei KH, Shu CF (2003) Chem Mater 11:2261
28. Tishchenko G, Bleha M (2005) J Membr Sci 248:45
29. Pyun J, Matyjaszewski K, Wu J, Kim GM, Mather SBPK (2003) Polymer 44:2739
30. Fu GD, Zong BY, Kang ET, Neoh KG, Lin CC, Liaw DJ (2004) Ind Eng Chem Res 43:6723
31. Chen YW, Wang W, Yu Z, Yuan ET, Kang KG, Neoh B, Krauter A (2004) Adv Funct Mater 14:471
32. Zhang C, Babonneau F, Bonmme C, Laine RM, Soles CL, Hristov HA, Yee AF (1998) J Am Chem Soc 120:8380